RSC Advances

PAPER

View Article Online
View Journal | View Issue

Cite this: *RSC Adv.*, 2026, **16**, 2241

A systematic comparison of density functional methods for determining spin-state energy gaps and spin transition temperature of spin crossover complexes

Esha Gera and Kuduva R. Vignesh *

In this paper, the spin-crossover (SCO) behavior of 26 transition metal complexes has been investigated by Density Functional Theory (DFT) using nine density functionals such as TPSS, BLYP, TPSSh, B3LYP, B3LYP*, OPBE, O3LYP, B3P86, and X3LYP, providing a comprehensive analysis of their effect towards computing spin-state energy gaps and spin transition temperature ($T_{1/2}$) of these SCO complexes. The SCO behavior of a complex highly depends on the free energy balance of high- and low-spin states, which is likewise influenced by physical properties including dispersion and vibrational entropy, which are all considered in the performed DFT calculations. Among all the tested functionals, the hybrid *meta*-GGA TPSSh functional and the B3LYP* functional predict the correct ground state and a reasonable HS–LS energy gap for all the SCO complexes. Their contemporary functionals, such as pure *meta*-GGA TPSS and GGA BLYP functionals, also predict the correct GS for all the complexes, but they overestimate the HS–LS gaps. Interestingly, the OPBE and the B3P86 functionals also predict the correct ground state for nearly 50% of the studied complexes. The TPSSh-predicted energy gap is in the proper range for SCO to occur in the majority of cases, including the SCO complexes with unusual geometry, and the $T_{1/2}$ predicted using this functional is also in good agreement with the experimental ones.

Received 12th December 2025
Accepted 22nd December 2025

DOI: 10.1039/d5ra09636g

rsc.li/rsc-advances

Introduction

Spin crossover (SCO) complexes are a fascinating class of coordination compounds that exhibit a remarkable change in their electronic spin state between high-spin and low-spin states but similar electronic energies in response to external stimuli such as temperature, pressure, or light. These complexes typically consist of first-row transition metal ions with the d^4–d^7 electronic configuration, coordinated to various organic ligands, significantly changing their magnetic and optical properties. Cambi and coworkers' pioneering work in the 1930s on the anomalous magnetism of iron(III) tris-derivatives of various bidentatedithiocarbamates resulted in the first detection of the interconversion of two spin states due to temperature change.[1–3] It was then defined that the SCO phenomenon originates from the competition between the crystal field splitting energy and the energy difference between different spin states of the metal ion. In the high-spin state, unpaired electrons occupy higher-energy orbitals due to weaker crystal field effects, whereas in the low-spin state, these electrons occupy lower-energy orbitals as a result of stronger crystal field splitting. Such a spin transition can lead to alterations in color, magnetic susceptibility, and other physical properties, making SCO complexes valuable in applications ranging from molecular switches to sensor devices.[4–7] Over the past few decades, advancements in the field have increased the number of metal centers and coordination settings capable of exhibiting this behavior. In particular, these SCO molecules have been used in metal–organic frameworks (MOFs) to create spin-crossover frameworks (SCOFs), which indeed became an ideal candidate for sensing applications.[8–13] Although interest in these systems continues to grow, for the recent experimental magnetic data limits the extent to which computational methods can be benchmarked and, consequently, constrains the rational design of spin-crossover materials with tailored electronic and structural characteristic,[14–18] however, such a benchmark study was exceptionally performed on 95 Fe(II) complexes very recently by Kulik and co-workers.[19] It is particularly challenging to construct a molecule with a specific transition temperature. The transition temperature ($T_{1/2}$), where the spin state of the complex changes from low-spin states to high-spin states, is a crucial factor in determining the physical properties of a system when both spin-state populations are equal. Understanding the factors influencing $T_{1/2}$ is crucial for harnessing these complexes for future technologies, including sensors, data storage, and molecular devices. In this regard,

Department of Chemical Sciences, Indian Institute of Science Education Research (IISER) Mohali, Sector-81, Knowledge City, S.A.S. Nagar, Mohali 140306, Punjab, India. E-mail: vigneshkuduvar@iisermohali.ac.in

significant advancements have been made in the field of computational modeling of SCO systems, and several approaches have been put forth to simulate the behavior of these systems, among which density functional theory (DFT) plays a crucial role. Because it is difficult to theoretically model SCO systems using *ab initio* methods such as CASSCF, CASPT2, NEVPT2, Coupled Cluster (CC), *etc.*, which can be used to precisely calculate the electronic energy difference between the two spin states,[20–23] whereas the DFT functionals were also found to predict these parameters correctly with reasonable computational cost.[24,25]

One key aspect in applying DFT to spin crossover complexes is the choice of exchange–correlation functional, for which the different exchange–correlation functionals, such as hybrid functionals, having different amounts of Hartree–Fock (HF) exchange, can influence the energy splitting between LS and HS states. We can explore how different molecular environments influence the spin state equilibrium and transition temperatures by systematically varying the amount of Hartree–Fock exchange in different hybrid functionals. To rationalize the effect of energy gaps of HS–LS and spin state equilibrium, we have chosen the combinations of pure DFT functionals, the mix of HF exchange and meta-generalised gradient approximation (GGA) exchange functionals, such as TPSS,[26] OPBE,[27] TPSSh,[28] O3LYP,[29] BLYP,[30] B3LYP*,[31,32] B3LYP,[33] B3P86,[34] and X3LYP[35] for this study. The selected exchange–correlation functionals are placed within the framework of Jacob's ladder in DFT.[36] The GGAs (OPBE, BLYP) represent the second rung, while TPSS belongs to the *meta*-GGA rung. The hybrid DFT functionals (B3LYP, B3LYP*, B3P86, O3LYP, X3LYP) and the hybrid *meta*-GGA functional TPSSh occupy higher rungs, as they incorporate fractions of exact HF exchange and, in some cases, additional semilocal ingredients. This hierarchical organization provides a systematic way to examine how the inclusion of gradient corrections, kinetic-energy density, and exact exchange affects the description of spin-crossover energetics. By benchmarking these functionals against experimental data, we evaluate the impact of increasing functional sophistication on spin-state energetics. The BLYP and OPBE are pure DFT functionals. TPSS is a pure *meta*-GGA functional, whereas TPSSh is a hybrid *meta*-GGA functional that incorporates 10% of the HF exchange functional. The B3LYP* hybrid functional is derived from the original B3LYP functional but modifies the amount of Hartree–Fock exchange to 15%, where the latter has 20% of HF exchange. Similarly, the O3LYP, B3P86, and X3LYP have HF exchange of 12%, 20%, and 21.8%, respectively. The difference between B3LYP and B3P86 is that B3LYP has 81% LYP GGA correlation, whereas B3P86 has 81% P86 GGA correlation; the amount of HF is the same for both the hybrid functional, *i.e.*, 20%. These functionals were chosen based on the previous reports, which predicted that DFT methods can improve spin-state energetics in iron systems (Fe^{II} and Fe^{III}) by incorporating 10% to 17% of HF exchange into the functional. Using some of these functionals, Ruiz and coworkers have performed a detailed analysis of a few SCO complexes[14] and rationalized that the hybrid *meta*-GGA functional TPSSh is the better one compared to other studied hybrid functionals for predicting the correct ground state as well as the transition temperature ($T_{1/2}$) value.[14] The B3LYP* has been designed to reproduce the HS–LS gap of Fe(III) complexes.[15] thus, these two functionals have been reconsidered for their tailored performance for Fe complexes and the implications for our study.

In this work, we have systematically studied twenty-six SCO complexes (including Cr^{II}, Mn^{III}, Mn^{II}, Fe^{III}, Fe^{II}, and Co^{II} metal ions with electronic configurations ranging from d^4 to d^7) having better transition temperature ($T_{1/2}$) as compared to their respective metal ions' SCO complexes reported to date. Using the above-mentioned functionals and rationalizing the effect of these functionals on the energy gaps of HS–LS, spin-pairing energy, spin density of metal and donor atoms, and ligand splitting of these SCO complexes. These recent SCO complexes were chosen to have a series of complexes with proven SCO behaviour including two-step transition temperature, good quality structures and a reasonably diverse ligand set to explore the impact of functional on these compounds (Fig. 1 and Table 1). To understand the source of functional performance in our computations, we have broken down the energy contributions, including exchange and correlation. If the calculation is compared to observed ground states, which reflect free energies, then one cannot ignore vibrational entropy, which largely determines the spin transition process. This entropy can be estimated decently but not very precisely from frequency analysis using standard quantum-chemical programs and is less sensitive to the DFT functional used.[3] To the best of our knowledge, except for a previously published study on other SCO compounds, this is the first systematic work that includes new functionals such as TPSS, BLYP, O3LYP, B3P86, and X3LYP, which were not studied earlier, and could predict the correct ground state for Cr(II), Mn(II), Co(II) and Mn(III) based SCO complexes as well.[14–19] Even though numerous benchmark studies on the accuracy of various exchange–correlation functionals to estimate energy differences between spin states and $T_{1/2}$ for Fe(II)/Co(II)-SCO systems have been published earlier, the origin of SCO of these complexes by bond parameters analysis, spin-pairing energy, and spin-density analysis were not explained in those studies which we additionally explained in this study.[14–19]

Computational details

The geometry optimizations were initiated from X-ray structures in the gas phase of all 26 complexes have been performed with different density functionals, such as TPSS,[26] OPBE,[27] TPSSh,[28] O3LYP,[29] BLYP,[30] B3LYP*,[31,32] B3LYP,[33] B3P86,[34] and X3LYP[35] using Gaussian 16. Although crystal packing, counterion interactions, and lattice vibrations are known to influence the thermodynamics of spin crossover in the solid state, gas-phase calculations provide a controlled framework to assess the intrinsic electronic preference of the isolated complex. This allows us to disentangle the fundamental performance of a functional in predicting spin-state energetics from external perturbations, ensuring that comparisons across different complexes are consistent and not biased by system-specific crystal environments. The fully optimized contracted def2-TZVP all-electron Gaussian basis set, developed by

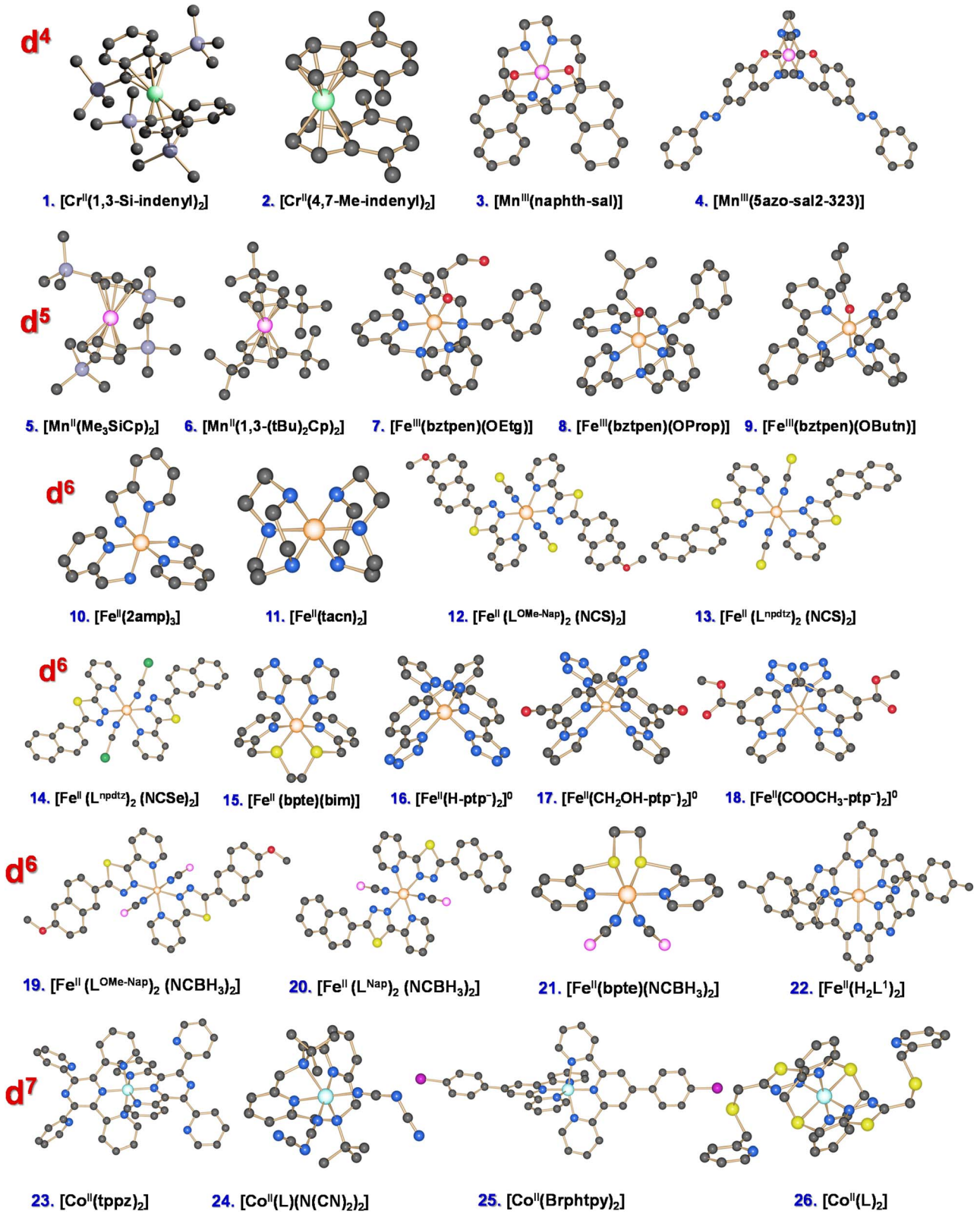

Fig. 1 Molecular structure of the 26 studied spin-crossover molecules. The solvent molecules, counteranions and H atoms were omitted for clarity. Color scheme: Cr(II): green; Mn (II/III): pink; Fe (II/III): orange; Co(II): light blue; O: red; N: blue; C: light grey; Br: dark pink; S: yellow; Se: green; B: light pink.

Table 1 Molecular formula and transition temperature of SCO systems studied in this work[a]

Complex no.	Molecular formula	Oxidation state of the metal center	Ref. code	d^n	$T_{1/2}$ (K)	Ref.
1	$[Cr(1,3\text{-Si-indenyl})_2]$	+2	MOSXEX	d^4	350	39
2	$[Cr(4,7\text{-Me-indenyl})_2]$	+2	—	d^4	250	40
3	[Mn(naphth-sal-1,5,8,12)]	+3	TUFXIE01	d^4	164	41
4	[Mn(5azo-sal2-323)](Cl)	+3	FEHKOW	d^4	560	42
5	$[Mn(Me_3SiCp)_2]$	+2	BUBGAH	d^5	125	43
6	$[Mn(1,3\text{-}(t\text{Bu})_2Cp)_2]$	+2	BUBGOV	d^5	314, 327	44
7	$[Fe(bztpen)(OEtg)](PF_6)_2$	+3	UGOLEJ	d^5	284	45
8	$[Fe(bztpen)(OButn)](PF_6)_2$	+3	UGOMIO	d^5	282	45
9	$[Fe(bztpen)(OProp)](PF_6)_2$	+3	UGOMUA	d^5	255	45
10	$[Fe(2amp)_3]Cl_2$	+2	FEPICC	d^6	196	46
11	$[Fe(tacn)_2](OTf)_2$	+2	DETTOL	d^6	330	47
12	$[Fe(L^{OMe\text{-}Nap})_2(NCS)_2]$	+2	LEYTAO	d^6	100	48
13	$[Fe\ (L^{npdtz})_2(NCS)_2]$	+2	VARDUR	d^6	110	49
14	$[Fe\ (L^{npdtz})_2(NCSe)_2]$	+2	VARFAZ	d^6	154	49
15	$[Fe(bpte)(bim)](ClO_4)_2$	+2	MEJVIJ	d^6	330	50
16	$[Fe(H\text{-}ptp^-)_2]^0$	+2	WILTES	d^6	296	51
17	$[Fe(CH_2OH\text{-}ptp^-)_2]^0$	+2	—	d^6	302	52
18	$[Fe(COOCH_3\text{-}ptp^-)_2]^0$	+2	LUTGEO	d^6	347	53
19	$[Fe(L^{OMe\text{-}Nap})_2(NCBH_3)_2]$	+2	LEYTIW	d^6	290	48
20	$[Fe(L^{Nap})_2(NCBH_3)_2]$	+2	LEYSUH	d^6	160, 300	48
21	$[Fe(bpte)(NCBH_3)_2]$	+2	GOSZUM	d^6	243	54
22	$[Fe(H_2L^1)_2]\ (BF_4)_2\cdot x(\text{solv.})$	+2	NIXWEZ	d^6	200	55
23	$[Co(L)_2]\ (ClO_4)_2$	+2	KAKTID	d^7	175	56
24	$[Co(L)(N(CN)_2)_2]$	+2	XUVQEN	d^7	238	57
25	$[Co(Brphtpy)_2](OTf)_2\cdot DMF\cdot 2H_2O$	+2	FICHAE	d^7	360	58
26	$[Co(tppz)_2](tcm)_2$	+2	HUCWIN	d^7	200	59

[a] Where, naphth-sal-*N*-1,5,8,12 = (2,2′-((1*E*,14*E*)-2,6,10,14-tetraazapentadeca-1,14-diene-1,15-diyl)diphenolate), 5azo-sal2-323 = 2,2′-((1*Z*,13*Z*)-2,6,9,13-tetraazatetradeca-1,13-diene-1,14-diyl)bis(4-((*E*)-phenyldiazenyl)phenolate), bztpen = *N*-benzyl-*N*,*N*′,*N*′-tris(2-pyridylmethyl) ethylenediamine, 1-OEtg = ethylene glycoxide, 1-OBu^n = *n*-butyl, 1-OProp = propyl, 2amp = 2-aminomethylpyridine, tacn = 1,4,7-triazacyclononane, $L^{OMe\text{-}Nap}$ = 2-(6-methoxynaphthalen-2-yl)-5-(pyridin-2-yl)-1,3,4-thiadiazole, L^{npdtz} = (2-naphthyl-5-pyridyl-1,2,4-thiadiazole), bpte = *S*,*S*′-bis(2-pyridylmethyl)-1,2-thioethane, bim = 2,2′-biimidazole, ptp = 2-(1*H*-pyrazol-1-yl)-6-(1*H*-tetrazol-5-yl)pyridine, H_2L^1 = 2-[5-(R-phenyl)-1*H*-pyrazole-3-yl] 6-benzimidazole pyridine, L = 2,5-bis[(2-pyridylmethyl)thio]methyl-1,3,4-thiadiazole, L(N(CN)$_2$) = *N*,*N*′-di-tertbutyl-2,11-diaza[3,3](2,6)pyridinophane, Brphtpy = 4′-(4-bromophenyl)-2,2′:6′,2″-terpyridine; OTf^- = trifluoromethanesulfonate, tppz = 2,3,5,6-tetrakis(2-pyridyl)pyrazine and tcm = tricyanomethanide anion.

Ahlrichs and co-workers, was employed for the metal ions Cr, Mn, Fe, Co, and heavier Se and Br atoms. For smaller atoms, such as S, O, C, N, and H, the 6-31G** basis set was used.[37,38] For all the functionals, Grimme's dispersion correction D3BJ has been implemented to consider weak interactions in the ligand environment by providing the necessary internal options in our calculations.[60,61] It is well known that the SCO phenomenon is highly temperature-dependent, where low temperatures favor the low-spin (LS) state and high temperatures favor the high-spin (HS) state. Furthermore, the SCO behavior is possible for any complexes when there should be a thermodynamic equilibrium between both the spin states, the low-spin (LS) and the high-spin (HS) state. To understand it further, we calculated the spin transition temperature ($T_{1/2}$) for all the complexes by computing the enthalpy change (ΔH) and entropy change (ΔS). For any ideal system, the Gibbs free energy change (ΔG) for the equilibrium of HS and LS states can be written as[62]

$$\Delta G = G^{HS} - G^{LS} = \Delta H - T\Delta S \quad (1)$$

When the populations of two spin states are in thermodynamic equilibrium, the ΔG becomes zero; thus, the transition temperature ($T_{1/2}$) can simply be calculated from the enthalpy and entropy changes using eqn (2).

$$T_{1/2} = \frac{\Delta H}{\Delta S} \quad (2)$$

This equation defines the enthalpy difference (ΔH) and entropy difference (ΔS) between the HS and LS states. These values were computed considering the zero-point energy correction changes and vibrational frequencies of the systems.

Results and discussion

Twenty-six mononuclear complexes comprising Cr^{II}, Mn^{III}, Mn^{II}, Fe^{II}, Fe^{III}, and Co^{II} spin-crossover systems were chosen to assess the precision of different DFT functionals in calculating the expected spin-state energy gaps, spin transition, and the correct ground state. These systems were chosen based on the criterion of the transition temperature. The experimental spin-transition values, as given in the respective references, along with the crystallographic chemical formula, are given in Table 1. A schematic illustration of every system under study is displayed in Fig. 1. Although DFT has been widely used to

calculate other physical parameters,[63–66] including exchange coupling constants,[67–69] it is still not easy to calculate the energy gaps between electronic states. The TPSSh functional has been extensively employed in SCO systems, with a primary focus on Fe(II) systems; however, its applicability to Cr^{II}, Mn^{III}, Mn^{II}, and Co^{II} SCO systems has not been extensively studied. Thus, we performed a benchmark study on these 26 complexes with other distinct functionals along with TPSSh. Structure optimizations were carried out for each of the chosen systems in both accessible spin states utilizing the OPBE, TPSS, BLYP, TPSSh, O3LYP, B3LYP*, B3LYP, B3P86, and X3LYP functionals.

Prediction of HS–LS gap by different functionals

The spin-state energy gap computed for all the complexes using nine different functionals is tabulated in Table S1, and the predicted GS can be visualized in Fig. 2, S1 and S2. The results that we observed for each functional are discussed below as follows:

OPBE. This pure DFT functional performs well in computing spin-state energy differences in SCO systems; however, its performance is insufficient for all systems. It predicted accurate spin ground state as low spin states for almost 50% of the complexes, which are **2**, **5**, **6**, **10**, **15**, **16**, **17**, **18**, **19**, **20**, **21**, **22**, **23**, **24**, and **26**, and their gap between the two spin states is found to be 3.2, 33.9, 25.2, 7.6, 16.3, 57.8, 55.7, 55.7, 11.9, 11, 19.5, 23.2, 31.3, 36.6 and 36.4 kJ mol^{-1}, respectively.

TPSS. This pure *meta*-GGA functional without HF exchange performs well in computing spin-state energy differences in SCO systems; however, its performance is not best for all systems. It predicted an accurate spin ground state, but it overestimated the energy window range to show SCO for all the complexes.

TPSSh. The TPSSh *meta*-GGA functional, which contains 10% of the HF exchange functional, predicts the correct ground state for all the complexes except for complex **24**.[54,57] Furthermore, the energy gap computed between the two spin states falls in the range of 0 to 33.4 kJ mol^{-1}, which is expected for a molecule to exhibit SCO behaviour for all the complexes.[14–19] It has been proven several times that the TPSSh functional works well for Fe(II) complexes. Interestingly, the TPSSh predicts the exact ground state and an energy gap for both the d^4 ions, such as Cr^{II} and Mn^{III} (complexes **1**–**4**), as well as for the d^7 Co^{II}

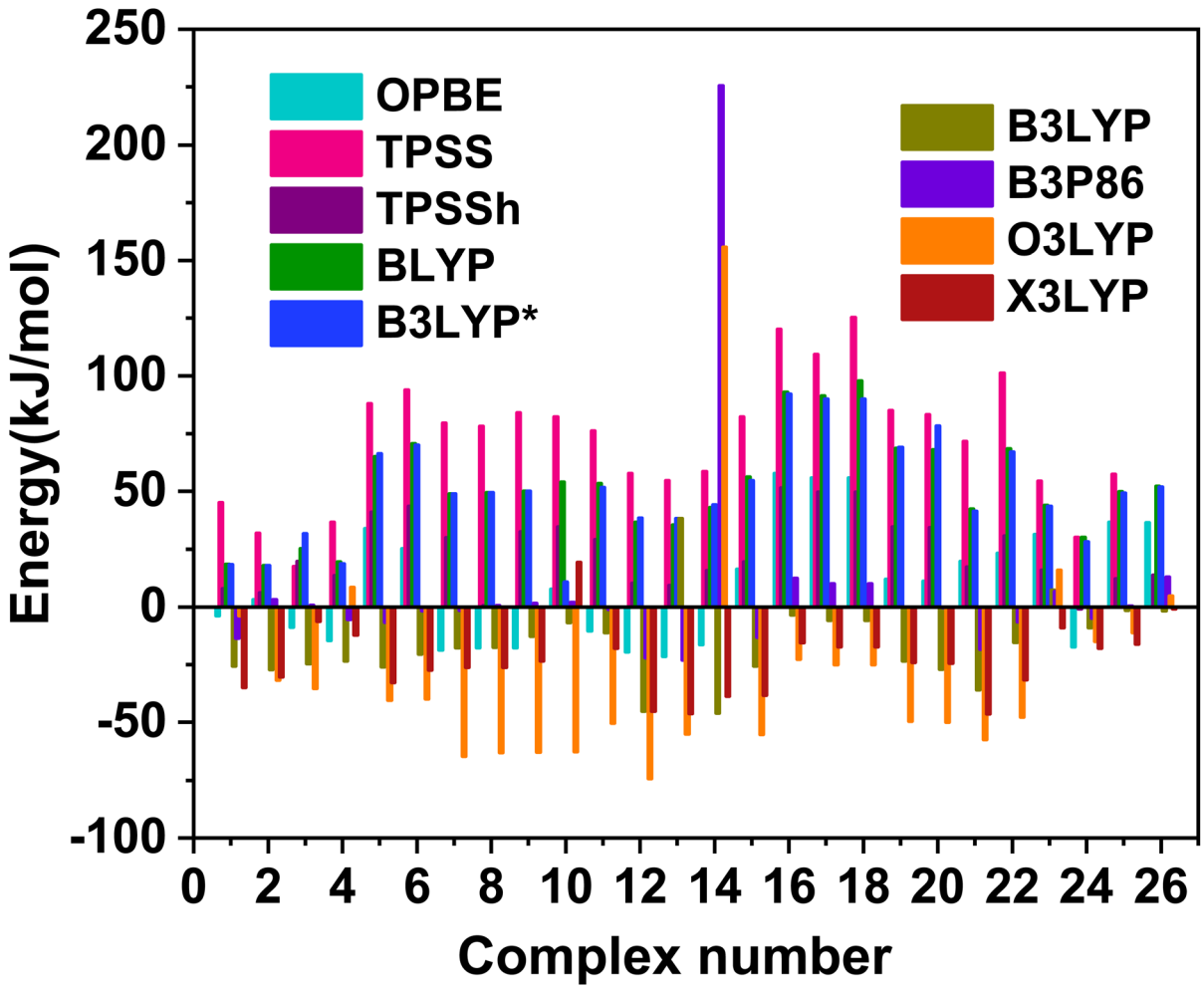

Fig. 2 Energy difference (HS–LS) for the 26 studied systems plotted for all nine hybrid functional methods: OPBE, TPSS, TPSSh, BLYP, B3LYP, B3LYP*, B3P86, O3LYP, and X3LYP.

complexes (Table S1 and Fig. 2).[14–19] However, for the Mn(II) complexes (**5** and **6**), and neutral Fe(II) complexes (**16**, **17**, and **18**) based on pyrazol-1-yl-6-(1*H*-tetrazol-5-yl) pyridine (ptp) ligand having a general formula of $[Fe^{II}(R\text{-}ptp^{-})_2]$, the gap between the two spin states is slightly overestimated and are found to be 40.9, 43.6, 51.4, 49.6, and 49.6 kJ mol^{-1} respectively. The overestimation of the energy gap for complexes **5**, **6**, **16**, **17**, and **18** and the incorrect GS prediction for complex **24** (a Co(II) complex, which also does not have any counterion) can be considered as a limitation of the performance of the TPSSh functional.

BLYP. This pure DFT functional also performs well in computing spin-state energy differences in SCO systems. It predicted an accurate spin ground state; however, it overestimated the energy gap to show SCO for all the complexes as the same as TPSS, but the gaps are comparatively less than the TPSS predicted ones.

B3LYP*. The B3LYP* hybrid functional with 15% HF exchange has predicted the accurate ground state for all the complexes. However, it overestimated the expected gap between HS–LS states for most of the complexes except for complexes **3** and **4** with d^4 (Mn^{III}), **10**, **15**, and **16** with d^6 (Fe^{II}), and **26** with d^7 (Co^{II}) configurations. The energy gap between the two spin states is calculated to be 31.6, 18.5, 10.7, and 28.1 kJ mol^{-1} for complexes **3**, **4**, **10**, and **24**, respectively.

B3LYP. The B3LYP functional contains 20% of HF exchange predicted HS state as the ground state for all the complexes except complexes **13** and **23**, for which it predicted the correct ground state. Among them, it predicted the correct ground state with a reasonable energy gap, *i.e.*, found to be 7.2 kJ mol^{-1} only for complex **23**, where the first coordination environment has an $\{N_4S_2\}$ donor environment.[54]

O3LYP. The O3LYP hybrid functional with 12% HF did not follow the expected trend; it was not even accurate in predicting the correct ground state, except for Co(II) complexes **23** and **26**, and their HS–LS gap is found to be 15.9 and 4.7 kJ mol^{-1}, respectively.

B3P86. The B3P86 functional, which contains 20% HF exchange, not previously studied for SCO complexes, accurately predicted the ground state for 50% of the chosen complexes. Importantly, the computed gap between the two spin states falls within the range of the energy window to show spin crossover for those complexes, such as **2**, **3**, **8**, **9**, **10**, **14**, **16**, **17**, **18**, **19**, **23**, **25**, and **26** and their energy gap for two spin states is calculated to be 3.2, 0.8, 0.6, 1.5, 1.9, 225.5, 12.2, 10, 10, 0.02, 6.7, 0.4, and 12.8 kJ mol^{-1} respectively. The energy gap predicted by the B3P86 hybrid functional is quite precise for showing spin crossover, except for complex **14**.

X3LYP. This hybrid functional predicted the HS state as the spin ground state for all the complexes except one complex, **10**, for which the energy difference between the two spin states is found to be 19.2 kJ mol^{-1}, which falls within the energy window of SCO behavior.

Comparison of TPSS *vs.* TPSSh. As is clear from Table S1 and Fig. 2, TPSS performs well in geometry optimisation and accurately predicts the ground state (GS), but it is not reliable for the energy gap, as it overestimates the energy gap, whereas TPSSh, which has a 10% HF exchange, reduces the self-interaction error present in the pure *meta*-GGA functional. So, it had improved spin-state energetics and orbital splitting predictions, because SCO energetics are very sensitive to the amount of exchange.

Comparison of BLYP, B3LYP* *vs.* B3LYP. To properly assess the role of Hartree–Fock exchange in spin-crossover calculations, the comparisons were made within the same functional family (*i.e.*, with identical exchange–correlation form). For instance, BLYP (0%), a modified B3LYP* (15%), and B3LYP with 20% exchange allow a direct evaluation of the HF exchange effect. The 'optimal' amount of HF exchange is necessarily functional dependent, and it plays a role in predicting the GS and the gap. As it is clear from Table S1 and Fig. 2, the pure DFT BLYP functional and the hybrid B3LYP* with less amount of HF exchange predict the correct GS, but they overestimate the energy gap. Whereas the hybrid B3LYP functional with a larger amount of HF exchange is not reliable in predicting the correct ground state, as well as the energy gap.

The TPSS, TPSSh, BLYP and B3LYP* functional worked well for most of the studied complexes, especially for Fe^{II} and Co^{II} systems; however, TPSS, BLYP, and B3LYP* overestimate the gap between the spin states, but B3LYP* is comparable with TPSSh rather than TPSS and BLYP. The reason behind is the presence of amount of HF exchange in TPSSh (10%) and B3LYP*(15%), whereas TPSS and BLYP are pure functionals.

Therefore, among all the functionals, the TPSSh and B3LYP* hybrid functionals (see Table S1, Fig. 2, S1 and S2) accurately predicted the ground state (low-spin) for most of the studied complexes and performed significantly better than the other functionals for all the systems, independent of the metal, d electron count, and oxidation state. Interestingly, when these two TPSSh and B3LYP* functionals overestimated the HS–LS gap, the B3P86 functional performed well for a family of neutral-charged iron(II) complexes **16**, **17**, and **18** based on pyrazol-1-yl-6-(1*H*-tetrazol-5-yl) pyridine (ptp) ligand. Thus, it is worth mentioning that, although this B3P86 is not widely used for the investigation of spin-crossover in transition metal complexes, it can be applied to charge-neutral Fe^{II} d^6 systems and some d^4 and d^5 molecules, as it predicts an accurate HS–LS gap. The OPBE functional performs well for some of the systems, especially with Cr(II), Mn(II), Fe(II), and Co(II) systems (see Table S1). However, it is useful for the complexes with a +2 oxidation state. The other functionals like O3LYP, B3LYP, and X3LYP stabilise mostly the high-spin state, making it more stable than the low-spin state. These observations suggest that the performance towards the representation of electronic energy differences in spin-crossover systems is better when the functional possesses only a small amount of HF exchange, with some exceptions for O3LYP.

Though the B3LYP* works better for Fe(III) systems, as per the earlier report,[15] but for the studied Fe(III) complexes, the TPSSh works better, and it is clear from Table S1 and Fig. 2. So, TPSSh still performs better compared to B3LYP*, for all the complexes, including Fe(III) systems. The energy gap value calculated using B3LYP* is almost double the value calculated using TPSSh. In contrast, B3LYP* is predicting the correct GS

and the expected energy gap for complex **24** $[Co^{II}(L)(N(CN)_2)_2]$, whereas TPSSh failed to predict its correct ground state.

Furthermore, the SCO complexes with Cr(II) and Mn(II) ions and an unusual geometry yielded similar results with all nine hybrid functionals, like other complexes, that BLYP, B3LYP*, TPSS, and TPSSh are reliable functionals for GS calculations, and TPSSh works better among all. On the other hand, the opposite result may occur if a hybrid functional mix has more HF exchange; however, B3P86 with 20% HF exceptionally predicts the correct ground state for some of the systems, which could be used for some cases. Fig. S1 and S2 display the energy differences between the two spin states (HS–LS) as a function of the exact exchange of Hartree–Fock content incorporated into the relevant functional for all the complexes.

Overall, across the 26-complex dataset, clear metal-dependent trends emerge in the reliability of hybrid functionals for SCO modelling. For the Cr(II) and Mn(II) systems, only the TPSSh provides ΔE(HS–LS) values closest to the window range expected for the SCO complexes, whereas TPSS, BLYP and B3LYP* predict correct GS for Cr and Mn systems, but overestimates the ΔE(HS–LS) values. Similarly, for Fe(II)/Fe(III)/Co(II) complexes, the TPSSh, TPSS, BLYP and B3LYP* functionals consistently reproduce correct GS, but only the TPSSh yields the reasonable spin-state gaps, except for one of the Co(II) complex. Interestingly, the B3P86 works well for some of the Fe(II)/Fe(III)/Co(II) complexes in predicting correct GS and the reasonable energy gaps.

Estimation of spin-transition temperature ($T_{1/2}$) by TPSSh, B3LYP*, and B3P86 functionals

We further computed the spin-transition temperatures ($T_{1/2}$) for all 26 complexes with TPSSh and B3LYP* since these functionals yielded the correct GS, and the same was computed with B3P86 functionals for the complexes it predicted the correct ground state. The computed quantitative $T_{1/2}$ values for the studied systems are presented in Fig. 3, Table S2 (TPSSh and B3P86), and S3 (B3LYP*).

TPSSh. The TPSSh functional predicts the $T_{1/2}$ values of 239 K, 266 K, 406 K, 574 K, 497 K, 164 K, 153 K, 229 K, 375 K, 399 K, 373 K, and 289 K for complexes **1**, **2**, **4**, **6**, **8**, **12**, **13**, **14**, **15**, **19**, **20**, **21**, and **25**, respectively which are in good agreement with the experimental $T_{1/2}$ values of 350, 250, 560 K, 327 K, 282 K, 100 K, 110 K, 330 K, 290 K, 300 K, 243 K, and 360 K, respectively. However, for complexes **3**, **5**, **7**, **9**, **10**, **11**, **16**, **17**, **18**, **22**, **23**, and **26**, it overestimates the $T_{1/2}$ values which are calculated to be 521 K, 724 K, 580 K, 570 K, 341 K, 558 K, 675 K, 664 K, 722 K, 361 K, 479 K, and 471 K. In contrast, the values were experimentally determined as 164 K, 125 K, 284 K, 255 K, 196 K, 330 K, 192 K, 296 K, 302 K, 347 K, 200 K, 175 K, and 200 K, respectively. The $T_{1/2}$ values were not computed using TPSSh for complex **20** since it did not predict the correct ground state.

B3LYP*. Since this hybrid functional predicts the correct ground state for all the complexes, transition temperature ($T_{1/2}$) values were calculated for all the complexes and are tabulated in Table S3. Only for complex **4**, the computed $T_{1/2}$ values are in good agreement with the experimental values, which are calculated to be 429 K. In contrast, the experimentally observed values are 560 K. However, it was discovered that the computed transition temperature values for the remaining complexes were overestimated compared to the experimental values.

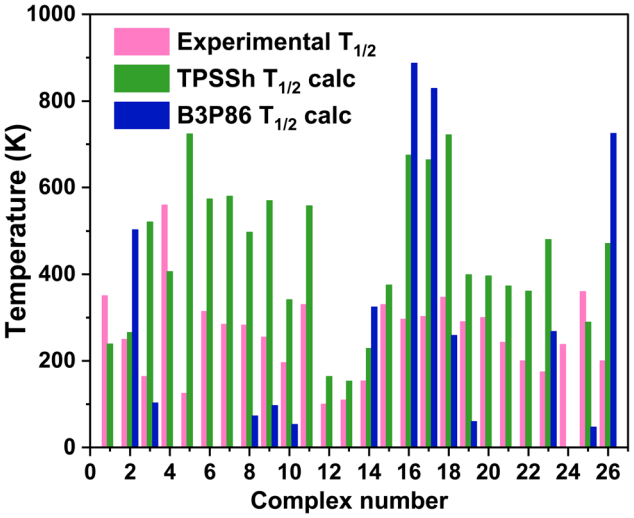

Fig. 3 Computed transition temperatures ($T_{1/2}$) in K for the 26 studied systems, using the TPSSh functional and 13 systems for which the B3P86 functional predicted correct GS, together with the experimental $T_{1/2}$ values.

B3P86. The $T_{1/2}$ values were also calculated for the B3P86 functional tabulated in Table S2, restricting it to 13 out of 26 complexes, since it correctly predicted the ground state for 13 of them. The computed transition temperature values for complexes **2**, **3**, **8**, **9**, **10**, **14**, **16**, **17**, **18**, **19**, **23**, **25**, and **26** are found to be 503 K, 103 K, 72 K, 97 K, 53 K, 324 K, 887 K, 829 K, 259 K, 60 K, 646 K, 47 K, and 725 K, whereas the experimentally calculated transition temperature values are 250 K, 164 K, 282 K, 255 K, 91 K, 154 K, 296 K, 302 K, 347 K, 290 K, 175 K, 360 K, and 200 K respectively. It is important to note that since these computed $T_{1/2}$ values are in good agreement with experimental ones, the B3P86 functional is also a good choice in predicting HS–LS gap and $T_{1/2}$ values for, particularly, SCO systems with charges, and d^6 and d^7 configurations.

From the above observation, one can be assured that the TPSSh is the best hybrid functional to compute the HS–LS gap as well as the $T_{1/2}$ value. Similarly, the B3P86 is also a better choice for predicting the $T_{1/2}$ value if it predicts the correct GS for some cases. As it is evident that the TPSSh is better functional in predicting an accurate ground state as well as yielding the $T_{1/2}$ values that are closer to the experimental $T_{1/2}$ values, we have further analyzed the optimized geometry of both spin states using TPSSh to derive how the computed bond parameters, spin density, and spin-pairing energies influence the $T_{1/2}$ values. The selected bond parameters for both the spin states, along with their X-ray structures, are shown in Tables S4 and S5. For all the complexes, the LS state's bond lengths are in good agreement with the X-ray structure parameters, which proves the presence of SCO behaviour of these complexes. Tables S6 and S7 present a comparison of computed and X-ray bond

parameters calculated using the B3LYP* and B3P86 functionals, respectively.

A comparison has been made for bond parameters computed using TPSSh, B3LYP*, and B3P86 functionals and the X-ray parameters, and we found that the TPSSh parameters have a better match with the X-ray bond parameters (Table S8). A slight deviation in the calculated bond parameters of the LS state from the X-ray structure could be rationalized by the exclusion of solvent and counter anions, which could affect the distortion in the coordination sphere. The M–O bond lengths of the LS state are slightly higher than those of HS in some complexes (for example, complex **3**), and this can be attributed to the use of room temperature X-ray structural data for optimising these states. Fig. 4 and S3 represent the bond parameters of the first coordination sphere atoms with the metal center.

Spin density analysis

The SCO behavior is highly dependent on the coordinated ligands, which facilitate the HS–LS transition if they are moderate ligand fields. To understand the role of ligands in these studied complexes and the donor atoms that are present in the first coordination environment, the spin density analysis was performed to see how a particular localisation of spin is occurring to promote the spin crossover using the TPSSh functional only. Fig. 5 and S4 show the spin density diagram for each complex with the TPSSh functional. Mulliken spin density

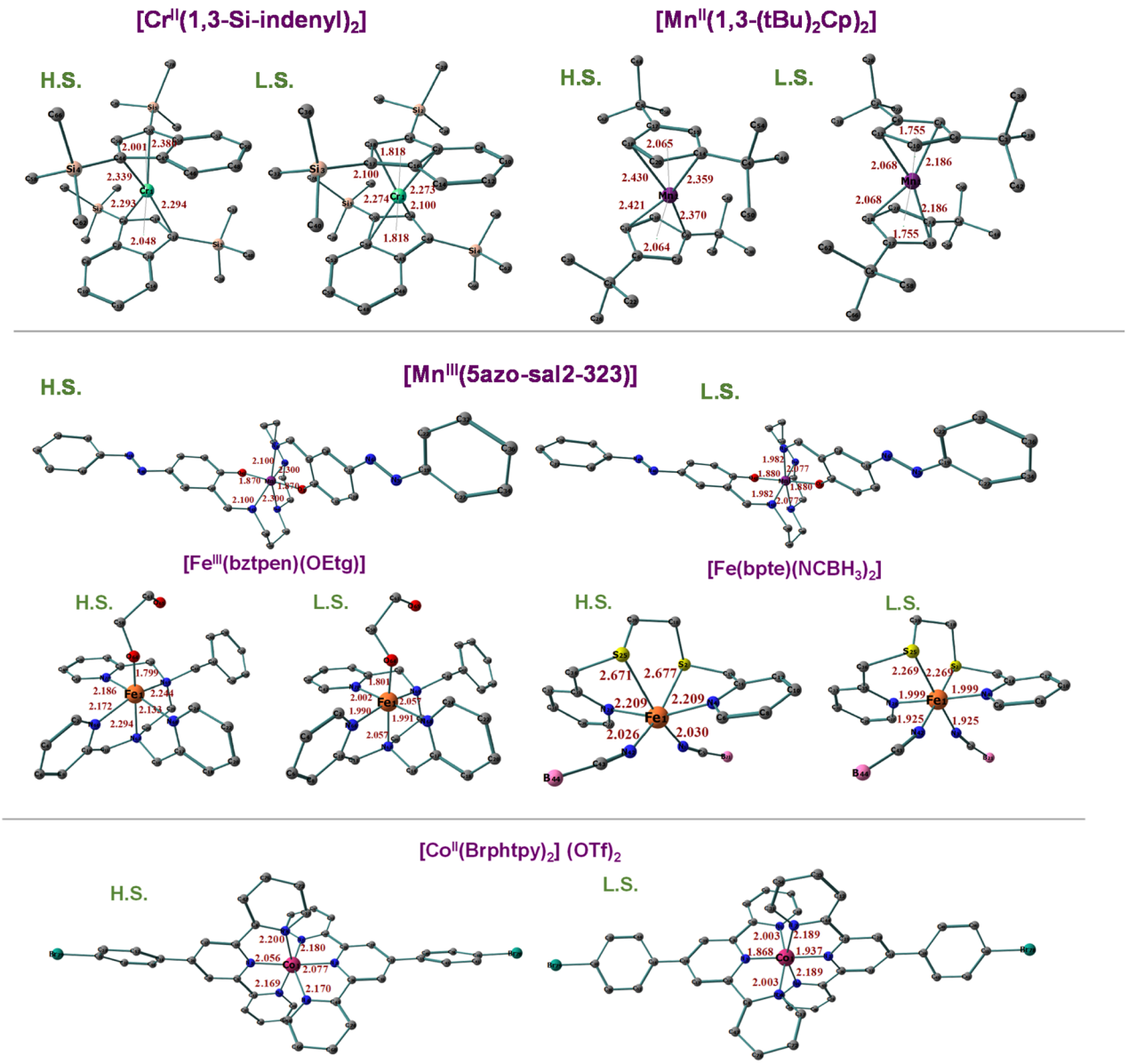

Fig. 4 Optimised structure of complexes (**2**)[Cr^{II}(1,3-Si-indenyl)$_2$], (**6**)[Mn^{II}(1,3-(^{t}Bu)$_2$Cp)$_2$], (**4**)[Mn^{III}(5azo-sal2-323)], (**7**)[Fe^{III}(bztpen)(OEtg)], (**21**)[Fe^{II}(bpte)(NCBH$_3$)$_2$], and (**25**)[Co^{II}(Brphtpy)$_2$] using the TPSSh functional and a few chosen bond values in the first coordination environment. The color code is as follows: orange, Fe, blue, N, red, O, grey, C, pink, B, yellow, S, green; Br, and hydrogen atoms are left out for clarity.

values of the metal centre and the first coordination environment atoms are mentioned in Table S9.

The spin density value of Mn^{III} ion in complexes **3** and **4** was found to be around *ca.* ~3.8 and ~1.99, respectively, for the HS; quintet state ($S = 2$), and LS; triplet state ($S = 1$). The lower spin value of the expected 4.0 for the HS Mn^{III} ion implies that the first coordination sphere atoms (N and O) of the ligand gain a spin density of *ca.* −0.008 to 0.036 for N atoms and *ca.* 0.0044 to 0.043 for O atoms through metal-to-ligand spin delocalization. The spin density value of the Fe^{III} ion in complexes **7**, **8**, and **9** is found to be *ca.* 4.04–4.07 for the Fe(III) metal center in the HS; sextet state ($S = 5/2$) and *ca.* 1.99 for LS; doublet state ($S = 1/2$). In these complexes, the spin density of N and O atoms in the first coordination sphere is found to be *ca.* 0.06–0.10 and *ca.* 0.42–0.47, respectively. Such large spin density values on the donor atoms can be explained by the σ-donor capacity at the alkoxide group, which increases with alkyl chain length, indicating an increase in the ligand field strength experienced by the Fe^{III} ion and, consequently, the stabilization of the LS state. Similarly, the Fe^{II} complexes with N_6 environment

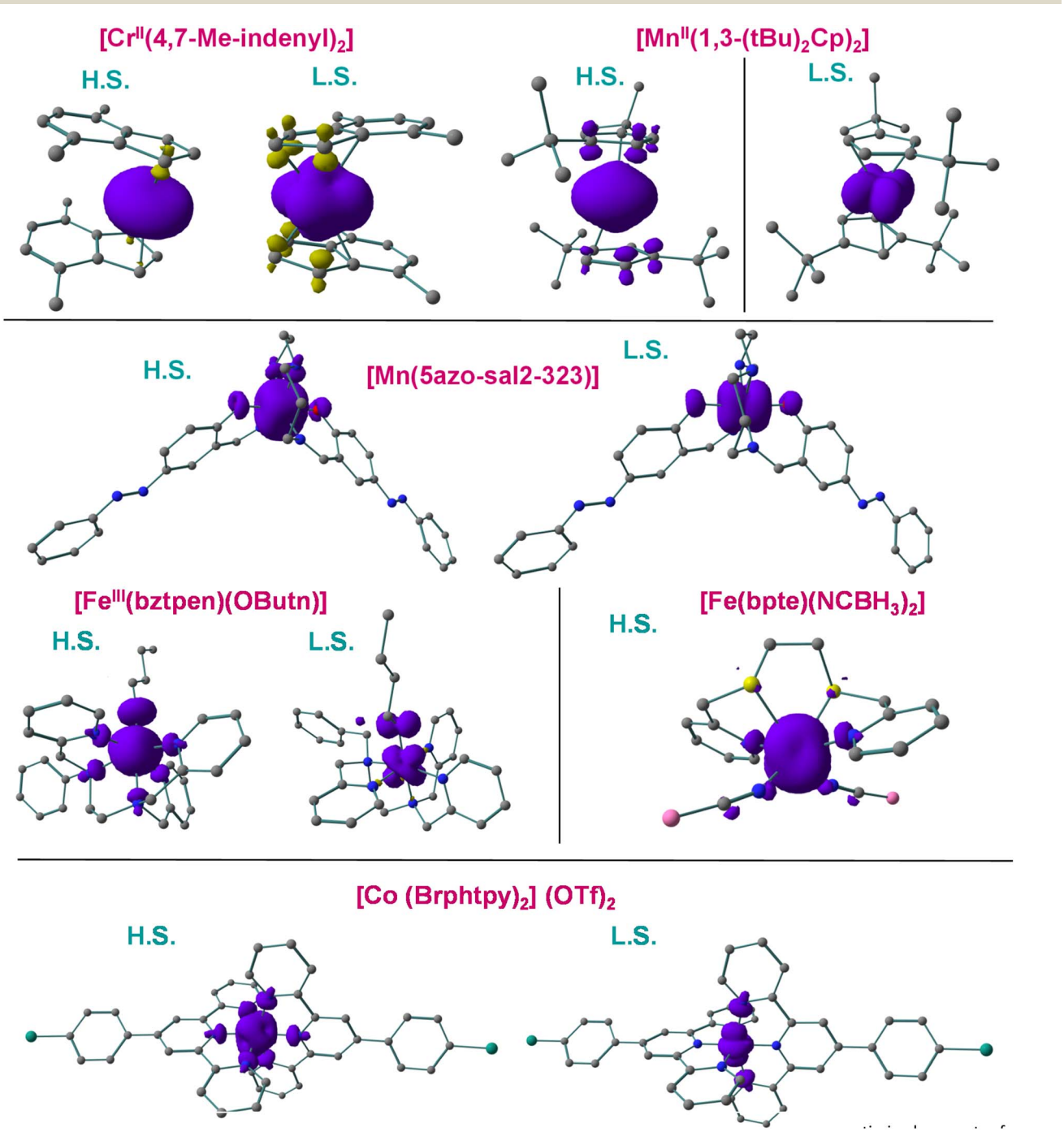

Fig. 5 Spin density diagram the contour value of 0.0043 e Å^{-3} for the optimized structure using with TPSSh optimized geometry for (**2**)[Cr^{II}(1,3-Si-indenyl)$_2$], (**6**)[Mn^{II}(1,3-(^{t}Bu)$_2$Cp)$_2$], (**4**)[Mn^{III}(5azo-sal2-323)], (**8**)[Fe^{III}(bztpen)(OButn)], (**21**)[Fe^{II}(bpte)(NCBH$_3$)$_2$], and (**25**)[Co^{II}(Brphtpy)$_2$].

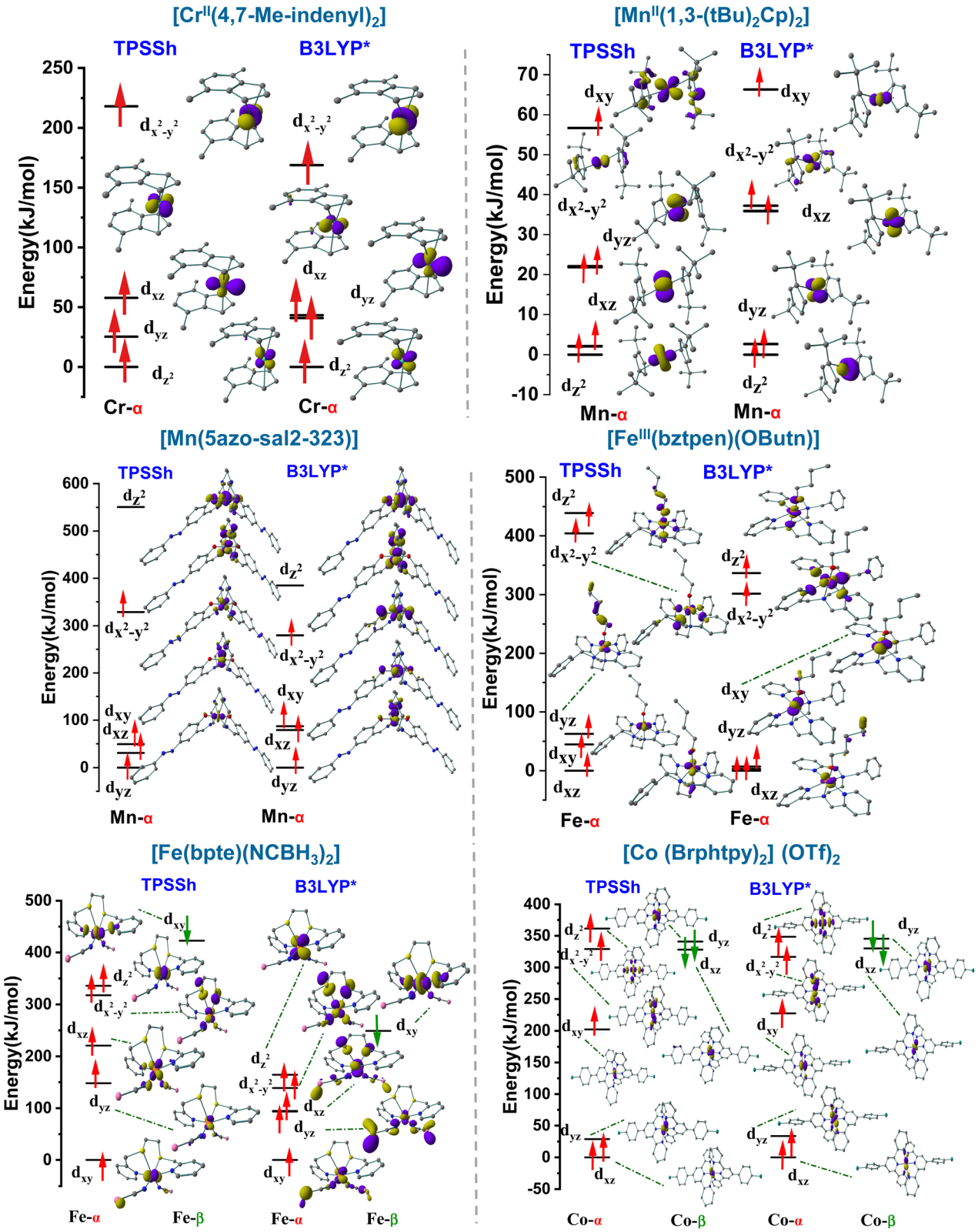

Fig. 6 d-Based eigenvalue plots for HS state computed with TPSSh and B3LYP* hybrid functionals for complexes (2)[Cr^{II}(1,3-Si-indenyl)$_2$], (6)[Mn^{II}(1,3-(^{t}Bu)$_2$Cp)$_2$], (4)[Mn^{III}(5azo-sal2-323)], (8)[Fe^{III}(bztpen)(OButn)], (21)[Fe^{II}(bpte)($NCBH_3$)$_2$], and (25)[Co^{II}(Brphtpy)$_2$]. Spin-up electrons (α) are represented by the red arrow, while those that are spin-down (β) are represented by the green arrow. The energy has scaled to the lowest spin-up orbitals for each scenario.

$[Fe^{II}(L^{npdtz})_2(NCX)_2]$; X = NCS^- (**13**), $NCSe^-$ (**14**) show the spin density of *ca.* 3.68 to 3.74 for the Fe(II) center. The nitrogen of the NCX derivative has a spin density of *ca.* 0.011 and 0.008 for NCS and NCSe, respectively, for HS, quintet state ($S = 2$). The presence of the X^- (S and Se) group (σ-donating ability decreases) causes a reduced spin density on the N atom of the NCX-group. These electronic differences show that the axial ligation can certainly have a considerable impact on the reported SCO characteristics in the Fe^{II} complexes. Other nitrogen atoms of the pyridine or naphthalene type propagate spin densities *via* spin polarisation; however, only a small amount of spin density is discovered in the NCS and NCSe groups. The σ-donating ability decrement ought to cause a shift in the SCO toward higher temperatures because the ligand field strength is known to fluctuate as $NCS^- < NCSe^-$; thus, an improvement in their computed $T_{1/2}$ values as follows (see Table S2). In all Co^{II} complexes, the spin density on the Co(II) ion is found to be *ca.* 2.68, for N atoms it is found to be *ca.* 0.032 to 0.06, and for the Br atom coordinated to the phenyl ring in **25** has a spin density of *ca.* −0.0004 to 0.001 for HS; quartet state ($S = 3/2$). Spin density for the Co(II) center in an LS state is found to be *ca.* 0.93, for N atoms, it is found to be *ca.* −0.014 to 0.06, and for the Br atom, it is found to be −0.0003 for an LS doublet state ($S = 1/2$) in complex **25**. This could be attributed to the presence of extra supramolecular contacts that promote SCO behavior, such as π–π interactions and halogen bonding.

The d-orbital splitting analysis

The temperature at which the SCO transition is observed is mainly determined by spin-state splitting and the associated free energy shift, since SCO is dependent on enthalpy and entropy contributions. Similarly, the orbital splitting and spin-pairing energy can significantly impact the spin ground state. Therefore, the d-based orbitals at their respective HS states have been computed to gain additional insight into the probability of spin-pairing energy. The eigenvalue plots with their energies are shown in Fig. 6 and S5 for all of the selected complexes. Since both TPSSh and B3LYP* functionals predict correct GS for all the complexes, the energy difference between the t_{2g}-like and e_g-like orbitals is computed with both the hybrid functionals TPSSh and B3LYP* and is mentioned in Table 2 with the electronic configurations. The estimation of the splitting between the t_{2g}-like and e_g-like orbitals was performed by identifying the frontier molecular orbitals corresponding to t_{2g} and e_g symmetry characters from the Kohn–Sham orbital manifold and measuring their relative separation within the same spin manifold, and not directly taking the absolute virtual orbital energies. The alpha and beta orbitals were considered based on the averaged separation for consistency for systems with more than half-filled and only alpha orbitals were considered for the systems with less than half-filled.[70] As it is clear from the observation of Table 2, the TPSSh computed energy gap between e_g and t_{2g} orbitals ($\Delta E = E_{eg} - E_{t_{2g}}$) for most of the complexes is closer to the minimum gap required for the spin

Table 2 d-Based electronic configuration in HS state and the energy difference between the e_g and t_{2g} orbitals in kJ mol^{-1} with both TPSSh and B3LYP* functionals for all 26 complexes

		$(\Delta E = E_{eg} - E_{t_{2g}})$ kJ mol^{-1}		
C. no.	Complexes	TPSSh	B3LYP*	Electronic configuration
1	$[Cr(1,3\text{-Si-indenyl})_2]$	75.7	183.8	$(d_{z^2})^1(d_{xz})^1(d_{yz})^1(d_{x^2-y^2})^1(d_{xy})^0$
2	$[Cr(4,7\text{-Me-indenyl})_2]$	218.1	168.7	$(d_{z^2})^1(d_{xz})^1(d_{yz})^1(d_{x^2-y^2})^1(d_{xy})^0$
3	[Mn(naphth-sal-1,5,8,12)]	279.2	192.4	$(d_{yz})^1(d_{xz})^1(d_{xy})^1(d_{x^2-y^2})^1(d_{z^2})^0$
4	[Mn(5azo-sal2-323)]	204.9	157.3	$(d_{xz})^1(d_{xy})^1(d_{yz})^1(d_{x^2-y^2})^1(d_{z^2})^0$
5	$[Mn(Me_3SiCp)_2]$	56.7	66.3	$(d_{z^2})^1(d_{xz})^1(d_{yz})^1(d_{x^2-y^2})^1(d_{xy})^1$
6	$[Mn(1,3\text{-}(^tBu)_2Cp)_2]$	100.9	72.8	$(d_{z^2})^1(d_{xz})^1(d_{yz})^1(d_{x^2-y^2})^1(d_{xy})^1$
7	$[Fe(bztpen)(OEtg)](PF_6)_2$	356.2	299.5	$(d_{xy})^1(d_{yz})^1(d_{xz})^1(d_{x^2-y^2})^1(d_{z^2})^1$
8	$[Fe(bztpen)(OButn)](PF_6)_2$	341.9	294.1	$(d_{xz})^1(d_{xy})^1(d_{yz})^1(d_{x^2-y^2})^1(d_{z^2})^1$
9	$[Fe(bztpen)(OProp)](PF_6)_2$	337.5	221.5	$(d_{xy})^1(d_{yz})^1(dx_z)^1(d_{x^2-y^2})^1(d_{z^2})^1$
10	$[Fe(2amp)_3]Cl_2$	84	73.8	$(d_{xz})^2(d_{yz})^1(d_{xy})^1(d_{x^2-y^2})^1(d_{z^2})^1$
11	$[Fe(tacn)_2](OTf)_2$	109.7	86.6	$(d_{xz})^2(d_{yz})^1(d_{xy})^1(d_{z^2})^1(d_{x^2-y^2})^1$
12	$[Fe(L^{OMe\text{-}Nap})_2(NCS)_2]$	63.7	83.7	$(d_{xy})^2(d_{xz})^1(d_{yz})^1(d_{x^2-y^2})^1(d_{z^2})^1$
13	$[Fe\ (L^{npdtz})_2(NCS)_2]$	63.4	84.2	$(d_{xy})^2(d_{xz})^1(d_{yz})^1(d_{x^2-y^2})^1(d_{z^2})^1$
14	$[Fe\ (L^{npdtz})_2(NCSe)_2]$	70.2	86.3	$(d_{xy})^2(d_{xz})^1(d_{yz})^1(d_{x^2-y^2})^1(d_{z^2})^1$
15	$[Fe(bpte)(bim)](ClO_4)_2$	101.7	86.6	$(d_{xy})^2(d_{yz})^1(d_{xz})^1(d_{z^2})^1(d_{x^2-y^2})^1$
16	$[Fe(H\text{-}ptp^-)_2]^0$	79.9	78.5	$(d_{xy})^2(d_{yz})^1(d_{xz})^1(d_{x^2-y^2})^1(d_{z^2})^1$
17	$[Fe(CH_2OH\text{-}ptp^-)_2]^0$	78.8	78.8	$(d_{xy})^2(d_{yz})^1(d_{xz})^1(d_{x^2-y^2})^1(d_{z^2})^1$
18	$[Fe(COOCH_3\text{-}ptp^-)_2]^0$	90.5	90.5	$(d_{xy})^2(d_{yz})^1(d_{xz})^1(d_{x^2-y^2})^1(d_{z^2})^1$
19	$[Fe(L^{OMe\text{-}Nap})_2(NCBH_3)_2]$	90.5	88.9	$(d_{xy})^2(d_{yz})^1(d_{xz})^1(d_{x^2-y^2})^1(d_{z^2})^1$
20	$[Fe(L^{Nap})_2(NCBH_3)_2]$	81.4	80.6	$(d_{xy})^2(d_{yz})^1(d_{xz})^1(d_{x^2-y^2})^1(d_{z^2})^1$
21	$[Fe(bpte)(NCBH_3)_2]$	96.7	44.2	$(d_{xy})^2(d_{yz})^1(d_{xz})^1(d_{x^2-y^2})^1(d_{z^2})^1$
22	$[Fe(H_2L^1)_2]\ (BF_4)_2 \cdot x(solv.)$	55.9	52.3	$(d_{xz})^2(d_{yz})^1(d_{xy})^1(d_{x^2-y^2})^1(d_{z^2})^1$
23	$[Co(L)_2]\ (ClO_4)_2$	188.5	121.9	$(d_{yz})^2(d_{xz})^2(d_{xy})^1(d_{x^2-y^2})^1(d_{z^2})^1$
24	$[Co(L)(N(CN)_2)_2]$	81.1	95.7	$(d_{yz})^2(d_{xy})^2(d_{xz})^1(d_{x^2-y^2})^1(d_{z^2})^1$
25	$[Co(Brphtpy)_2](OTf)_2 \cdot DMF \cdot 2H_2O$	126.9	89.4	$(d_{xz})^2(d_{yz})^2(d_{xy})^1(d_{x^2-y^2})^1(d_{z^2})^1$
26	$[Co(tppz)_2](tcm)_2$	132.3	106.6	$(d_{yz})^2(d_{xz})^2(d_{xy})^1(d_{x^2-y^2})^1(d_{z^2})^1$

pairing to occur (~240 kJ mol^{-1});[71–73] Thus, only the TPSSh computed values are taken for further discussion.

For Fe^{II} and Co^{II} complexes, the energy difference between the t_{2g}-like and e_g-like orbitals is 50–130 kJ mol^{-1}. For Mn^{III} and Fe^{III} complexes, it is 200–300 kJ mol^{-1}, and for Cr^{II} and Mn^{II} complexes, it is 70–200 kJ mol^{-1}. This splitting energy makes it richly evident that structural alterations brought about by ligands drastically impact the energy levels and, consequently, the complexes' SCO characteristics. Electron pairing in the t_{2g} orbitals is necessary for the formation of the LS complex, and axial NCX^- ligation along with N_4 donor ligands compared to the axial N ligation of the N_6 ligands has a significant impact on both orbitals (in most of the Fe^{II} and Co^{II} complexes) to facilitate spin pairing (spin transfer between e_g and t_{2g} orbitals, which refers to how electrons redistribute between these orbitals during the transition between HS and LS states) under certain thermodynamic conditions.[74,75] This lends confidence to the theory that axial ligation can help to reduce the energy gap between e_g and t_{2g} orbitals, along with that ligands with moderate-to-weak π-type interactions are most suited for observing SCO features[76]

Conclusion

In this work, twenty-six spin-crossover complexes were optimized using density functional theory (DFT) with the key aim being the computation of finding a suitable functional in predicting the exact spin ground state, transition temperature, spin-pairing energy, and probing the origin of SCO behavior in those systems. We have chosen TPSSh and B3LYP* functionals, which are well-known in predicting the correct GS and other functionals such as TPSS, BLYP, OPBE, O3LYP, B3LYP, B3P86, and X3LYP for this study. Below is a summary of the findings from this study.

(1) A variety of complexes with different types of asymmetric units having counterions, solvent molecules, neutral charged, two-step transition temperature complex, and unusual SCO behaviour were chosen to study the consistency of the particular hybrid functional in predicting an accurate spin ground state as well as the transition temperature, even with their isolated molecule. Our calculations mostly reproduce these values to maintain consistency across the dataset.

(2) Functionals with higher HF exchange (B3LYP, B3P86, and X3LYP) sometimes yield correct spin-state energetics, but the HS–LS gaps are overestimated. Functional like OPBE usually predicts LS or HS states reasonably well for molecules that are highly dependent on the correlation effects. Hybrid functionals with moderate HF exchange, like B3LYP* or TPSSh, often strike a balance, making them suitable for systems with moderate electronic character.

(3) In comparison of meta GGA functionals, TPSS overestimated the energy gap as compared to TPSSh; similarly, in GGA functionals, BLYP overestimated the energy gap as compared to B3LYP*. But all four functionals predicted correct GS.

(4) TPSSh (10% HF exchange) and B3LYP* (15% HF exchange) are widely used for SCO systems, providing reasonable energy gaps for our studied systems, too. The expected electronic energy differences between the two spin states for an SCO, which is less than 33.4 kJ mol^{-1}, computed using these functionals, mostly fall in this range. However, B3LYP* overestimates the HS–LS gap as well as the $T_{1/2}$ values for a few complexes.

(5) Remarkably, for about 50% of the studied complexes, the pure DFT functional OPBE and the B3P86 functional with large HF exchange (20%) also predict the exact ground state. Moreover, the B3P86 computed $T_{1/2}$ values are in good agreement with experimental ones, which hints that the B3P86 functional is also an excellent candidate for predicting HS–LS gap and $T_{1/2}$ values for SCO systems containing charge ligands, as well as d^6 and d^7 configurations.

(6) It is evident that the hybrid *meta*-GGA functional TPSSh, in conjunction with the def2 triple-ζ quality basis set featuring polarisation functions, can predict accurate ground state, energy gap, transition temperature $T_{1/2}$ value, and spin pairing energy for the electronic d^4 to d^7 configurations (Mn^{III}, Fe^{III}, Fe^{II}, and Co^{II}). The overestimation of the energy gap for complexes **5**, **6**, **16**, **17**, and **18** and the incorrect GS prediction for a Co(II) complex (**24**), which does not have a counteranion, can be realised as a limitation of the performance of the TPSSh functional.

Conflicts of interest

There are no conflicts to declare.

Data availability

The data supporting this article, such as Density Functional Theory (DFT) optimized structures, structural parameters of those complexes, DFT computed electronic energies, spin densities, spin-pairing energies, energy gap of ground and excited states, and transition temperatures, have been included as part of the supplementary information (SI). Supplementary information: energy gap figures, tables, and figures related to spin density analysis and bond parameter. See DOI: https://doi.org/10.1039/d5ra09636g.

Acknowledgements

Esha Gera thanks CSIR for providing a PhD fellowship. K. R. V. thanks the IISER Mohali-High Performing Computing Facility for providing computing resources and also thanks SERB for providing start-up research grant funding (SRG/2023/000286).

Notes and references

1 L. Cambi and L. Szegö, *Ber. Dtsch. Chem. Ges.*, 1931, **64**, 2591–2598.
2 L. Cambi and L. Malatesta, *Ber. Dtsch. Chem. Ges.*, 1937, **70**, 2067–2078.
3 K. P. Kepp in *The Electronic Determinants of Spin Crossover Described by Density Functional Theory*, ed. E. Broclawik, T.

Borowski and M. Radoń, Springer International Publishing, Cham, 2019, pp. 1–33.
4 A. Bousseksou, G. Molnár and G. Matouzenko, *Eur. J. Inorg. Chem.*, 2004, **2004**, 4353–4369.
5 O. Kahn and C. J. Martinez, *Science*, 1998, **279**, 44–48.
6 M. S. Alam, M. Stocker, K. Gieb, P. Müller, M. Haryono, K. Student and A. Grohmann, *Angew. Chem., Int. Ed.*, 2010, **49**, 1159–1163.
7 N. T. Madhu, S. Ivan, S. Frank, K. Svetlana, F. Olaf and R. Mario, *C. R. Chim.*, 2008, **11**, 1166–1174.
8 J. Cirera, *Rev. Inorg. Chem.*, 2014, **34**, 199–216.
9 G. J. Halder, C. J. Kepert, B. Moubaraki, K. S. Murray and J. D. Cashion, *Science*, 2002, **298**, 1762–1765.
10 P. D. Southon, L. Liu, E. A. Fellows, D. J. Price, G. J. Halder, K. W. Chapman, B. Moubaraki, K. S. Murray, J.-F. Létard and C. J. Kepert, *J. Am. Chem. Soc.*, 2009, **131**, 10998–11009.
11 A. Martínez-Martinez, S. Gullace, E. Resines-Urien, L. Martín-Pérez, J. Collado, R. Arranz, E. Burzuri, C. Santiago, E. C. Sañudo and J. S. Costa, *Small*, 2024, 2408966.
12 J. de Jesus Velazquez-Garcia, K. Basuroy, J. Wong, S. Demeshko, F. Meyer, I. Kim, R. Henning, Y. U. Staechelin, H. Lange and S. Techert, *Chem. Sci.*, 2024, **15**, 13531–13540.
13 N. El Islam Belmouri, C. Cazelles, J. Linares and K. Boukheddaden, *Eur. J. Inorg. Chem.*, 2024, **27**, e202400475.
14 J. Cirera, M. Via-Nadal and E. Ruiz, *Inorg. Chem.*, 2018, **57**, 14097–14105.
15 D. Vidal, J. Cirera and J. Ribas-Arino, *Dalton Trans.*, 2021, **50**, 17635–17642.
16 S. Gómez-Coca and E. Ruiz, *Dalton Trans.*, 2024, **53**, 11895–11902.
17 K. P. Kepp, *Inorg. Chem.*, 2016, **55**, 2717–2727.
18 O. S. Siig and K. P. Kepp, *J. Phys. Chem. A*, 2018, **122**, 4208–4217.
19 V. Vennelakanti, M. G. Taylor, A. Nandy, C. Duan and H. J. Kulik, *Chem. Phys. Lett.*, 2023, **159**, 024120.
20 S. Vancoillie, H. Zhao, M. Radoń and K. Pierloot, *J. Chem. Theory Comput.*, 2010, **6**, 576–582.
21 K. Pierloot, Q. M. Phung and A. Domingo, *J. Chem. Theory Comput.*, 2017, **13**, 537–553.
22 S. Roy Chowdhury, N. Nguyen and B. Vlaisavljevich, *J. Phys. Chem. A*, 2023, **127**, 3072–3081.
23 M. Radoń, G. Drabik, M. Hodorowicz and J. Szklarzewicz, *Chem. Sci.*, 2024, **15**, 20189–20204.
24 A. Vargas, I. Krivokapic, A. Hauser and L. M. Lawson Daku, *Phys. Chem. Chem. Phys.*, 2013, **15**, 3752–3763.
25 S. Gómez-Coca and E. Ruiz, *Inorg. Chem.*, 2024, **63**, 13338–13345.
26 J. Tao, J. P. Perdew, V. N. Staroverov and G. E. Scuseria, *Phys. Rev. Lett.*, 2003, **91**, 146401.
27 N. C. Handy and A. J. and Cohen, *Mol. Phys.*, 2001, **99**, 403–412.
28 J. P. K. Doye and F. Calvo, *Chem. Phys. Lett.*, 2003, **119**, 12680–12681.
29 W.-M. Hoe, A. J. Cohen and N. C. Handy, *Chem. Phys. Lett.*, 2001, **341**, 319–328.
30 B. Miehlich, A. Savin, H. Stoll and H. Preuss, *Chem. Phys. Lett.*, 1989, **157**, 200–206.
31 M. Reiher, *Inorg. Chem.*, 2002, **41**, 6928–6935.
32 M. Reiher, O. Salomon and B. Artur Hess, *Theor. Chem. Acc.*, 2001, **107**, 48–55.
33 A. D. Becke, *Chem. Phys. Lett.*, 1993, **98**, 5648–5652.
34 F. Abu-Awwad and P. Politzer, *J. Comput. Chem.*, 2000, **21**, 227–238.
35 X. Xu and W. A. Goddard, *Proc. Natl. Acad. Sci. U. S. A.*, 2004, **101**, 2673–2677.
36 J. P. Perdew and K. Schmidt, *AIP Conf. Proc.*, 2001, **577**, 1–20.
37 J. Laun, D. Vilela Oliveira and T. Bredow, *J. Comput. Chem.*, 2018, **39**, 1285–1290.
38 V. A. Rassolov, M. A. Ratner, J. A. Pople, P. C. Redfern and L. A. Curtiss, *J. Comput. Chem.*, 2001, **22**, 976–984.
39 E. D. Brady, J. S. Overby, M. B. Meredith, A. B. Mussman, M. A. Cohn, T. P. Hanusa, G. T. Yee and M. Pink, *J. Am. Chem. Soc.*, 2002, **124**, 9556–9566.
40 M. B. Meredith, J. A. Crisp, E. D. Brady, T. P. Hanusa, G. T. Yee, M. Pink, W. W. Brennessel and V. G. Young, Jr., *Organometallics*, 2008, **27**, 5464–5473.
41 S.-Z. Zhao, C.-Y. Qin, S. Wang, M. Yamashita, Y.-H. Li and W. Huang, *Dalton Trans.*, 2020, **49**, 4293–4305.
42 S. Ghosh, S. Bagchi, S. Kamilya, S. Mehta, D. Sarkar, R. Herchel and A. Mondal, *Dalton Trans.*, 2022, **51**, 7681–7694.
43 N. Hebendanz, F. H. Koehler, G. Mueller and J. Riede, *J. Am. Chem. Soc.*, 1986, **108**, 3281–3289.
44 M. D. Walter, C. D. Sofield, C. H. Booth and R. A. Andersen, *Organometallics*, 2009, **28**, 2005–2019.
45 N. Ortega-Villar, A. Y. Guerrero-Estrada, L. Piñeiro-López, M. C. Muñoz, M. Flores-Álamo, R. Moreno-Esparza, J. A. Real and V. M. Ugalde-Saldívar, *Inorg. Chem.*, 2015, **54**, 3413–3421.
46 K. W. Törnroos, M. Hostettler, D. Chernyshov, B. Vangdal and H.-B. Bürgi, *Chem.–Eur. J.*, 2006, **12**, 6207–6215.
47 A. S. Tolla, A. Banerjee, S. Stjepanovic, J. Li, W. W. Brennessel, R. Loloee and F. A. Chavez, *Eur. J. Inorg. Chem.*, 2013, **2013**, 2115–2121.
48 S. Sundaresan, J. Kiehl, L. M. Carrella and E. Rentschler, *Cryst. Growth Des.*, 2023, **23**, 1648–1655.
49 J. Kiehl, T. Hochdörffer, L. M. Carrella, V. Schünemann, M. H. Nygaard, J. Overgaard and E. Rentschler, *Inorg. Chem.*, 2022, **61**, 3141–3151.
50 S. Yergeshbayeva, J. J. Hrudka, J. Lengyel, R. Erkasov, S. A. Stoian, A. Dragulescu-Andrasi and M. Shatruk, *Inorg. Chem.*, 2017, **56**, 11096–11103.
51 B. Schäfer, C. Rajnák, I. Šalitroš, O. Fuhr, D. Klar, C. Schmitz-Antoniak, E. Weschke, H. Wende and M. Ruben, *Chem. Commun.*, 2013, **49**, 10986–10988.
52 K. Senthil Kumar, S. Vela, B. Heinrich, N. Suryadevara, L. Karmazin, C. Bailly and M. Ruben, *Dalton Trans.*, 2020, **49**, 1022–1031.
53 K. Senthil Kumar, I. Šalitroš, B. Heinrich, O. Fuhr and M. Ruben, *J. Mater. Chem. C*, 2015, **3**, 11635–11644.
54 A. Arroyave, A. Lennartson, A. Dragulescu-Andrasi, K. S. Pedersen, S. Piligkos, S. A. Stoian, S. M. Greer, C. Pak,

O. Hietsoi, H. Phan, S. Hill, C. J. McKenzie and M. Shatruk, *Inorg. Chem.*, 2016, **55**, 5904–5913.
55 R. Saiki, H. Miyamoto, H. Sagayama, R. Kumai, G. N. Newton, T. Shiga and H. Oshio, *Dalton Trans.*, 2019, **48**, 3231–3236.
56 F. Fürmeyer, D. Münzberg, L. M. Carrella and E. Rentschler, *Molecules*, 2020, **25**, 855.
57 S. Ghosh, S. Selvamani, S. Mehta and A. Mondal, *Dalton Trans.*, 2020, **49**, 9208–9212.
58 Y. Zhou, X.-Q. Wei, Y. Gu, Q.-Q. Zhao and D. Shao, *Eur. J. Inorg. Chem.*, 2023, **26**, e202200666.
59 J. Palion-Gazda, A. Świtlicka-Olszewska, B. Machura, T. Grancha, E. Pardo, F. Lloret and M. Julve, *Inorg. Chem.*, 2014, **53**, 10009–10011.
60 S. Grimme, J. Antony, S. Ehrlich and H. Krieg, *Chem. Phys. Lett.*, 2010, **132**, 154104.
61 S. Grimme, S. Ehrlich and L. Goerigk, *J. Comput. Chem.*, 2011, **32**, 1456–1465.
62 P. Gütlich, H. Köppen, R. Link and H. G. Steinhäuser, *Chem. Phys. Lett.*, 1979, **70**, 3977–3983.
63 I. Georgieva, N. Trendafilova, T. Zahariev, N. Danchova and S. Gutzov, *J. Lumin.*, 2018, **202**, 192–205.
64 V. V. Syakaev, A. N. Masliy, S. N. Podyachev, S. N. Sudakova, A. E. Shvedova, I. I. Lentin, A. N. Gorbunov, I. M. Vatsouro, D. V. Lapaev, G. Sh. Mambetova, V. V. Kovalev, A. M. Kuznetsov and A. R. Mustafina, *Inorg. Chim. Acta*, 2024, **561**, 121848.
65 M. van der Meer, S. Manck, S. Sobottka, S. Plebst and B. Sarkar, *Organometallics*, 2015, **34**, 5393–5400.
66 M. Uudsemaa and T. Tamm, *J. Phys. Chem. A*, 2003, **107**, 9997–10003.
67 L. Fohlmeister, K. R. Vignesh, F. Winter, B. Moubaraki, G. Rajaraman, R. Pöttgen, K. S. Murray and C. Jones, *Dalton Trans.*, 2015, **44**, 1700–1708.
68 K. R. Vignesh, S. K. Langley, K. S. Murray and G. Rajaraman, *Chem.–Eur. J.*, 2015, **21**, 2881–2892.
69 K. R. Vignesh, S. K. Langley, C. J. Gartshore, B. Moubaraki, K. S. Murray and G. Rajaraman, *Inorg. Chem.*, 2017, **56**, 1932–1949.
70 R. J. Deeth, *Faraday Discuss.*, 2003, **124**, 379–391.
71 V. Mishra, R. Mukherjee, J. Linares, E. Codjovi, F. Varret and M. Lawson-Daku, *ICAME 2007*, Berlin, Heidelberg, 2009, pp. 1305–1312.
72 A. Bousseksou, G. Molnár, L. Salmon and W. Nicolazzi, *Chem. Soc. Rev.*, 2011, **40**, 3313–3335.
73 A. Hauser, *Chem. Phys. Lett.*, 1986, **124**, 543–548.
74 S. Sundaresan, J. Eppelsheimer, E. Gera, L. Wiener, L. M. Carrella, K. R. Vignesh and E. Rentschler, *Dalton Trans.*, 2024, **53**, 10303–10317.
75 W. Phonsri, D. S. Macedo, K. R. Vignesh, G. Rajaraman, C. G. Davies, G. N. L. Jameson, B. Moubaraki, J. S. Ward, P. E. Kruger, G. Chastanet and K. S. Murray, *Chem.–Eur. J.*, 2017, **23**, 7052–7065.
76 M. Schmidt, D. Wiedemann, B. Moubaraki, N. F. Chilton, K. S. Murray, K. R. Vignesh, G. Rajaraman and A. Grohmann, *Eur. J. Inorg. Chem.*, 2013, **2013**, 958–967.